

# UniAttn: Reducing Inference Costs via Softmax Unification for Post-Training LLMs

Yizhe Xiong<sup>1</sup>, Wei Huang<sup>2</sup>, Xin Ye<sup>3</sup>, Hui Chen<sup>1</sup>, Zijia Lin<sup>1</sup>, Haoran Lian<sup>4</sup>  
Zhenpeng Su<sup>3</sup>, Jungong Han<sup>5</sup>, Guiguang Ding<sup>1</sup>

<sup>1</sup>School of Software, Tsinghua University

<sup>2</sup>School of Computer Science, Beijing University of Posts and Telecommunications

<sup>3</sup>Kuaishou Technology <sup>4</sup>Beihang University

<sup>5</sup>Department of Automation, Tsinghua University  
xiongyizhe2001@gmail.com

## Abstract

Post-training is essential for adapting Large Language Models (LLMs) to real-world applications. Deploying post-trained models faces significant challenges due to substantial memory overhead and noticeable inference latency. Existing work has identified significant redundancies in LLMs and proposed efficient architectures, namely intra-layer KV sharing and cross-layer KV sharing. However, intra-layer KV sharing still results in high inference costs, while cross-layer KV sharing leads to significant performance degradation. As a result, both methods remain suboptimal for post-training pre-trained LLMs. In this paper, we identify that the Softmax operation is a primary bottleneck for LLM inference and discover that it is actually highly redundant during post-training. We propose Softmax **Unification in Attention (UniAttn)**, a novel post-training method that unifies Softmax activations across transformer blocks to reduce LLM inference costs. Additionally, UniAttn adopts a linear projection to compensate for the errors induced by Softmax unification. Experiments show that UniAttn matches the performance of standard post-training while significantly reducing inference costs, outperforming existing efficient architectures during post-training. Our code will be available at <https://github.com/Bostoncake/UniAttn>.

## 1 Introduction

Post-training (Lambert et al., 2024) has become a critical step in developing advanced LLMs for both general-purpose tasks (OpenAI, 2023; Liu et al., 2023) and domain-specific tasks (Thirunavukarasu et al., 2023; Wu et al., 2023; Shao et al., 2024). It typically refers to performing supervised fine-tuning (SFT), reinforcement learning or even domain-specific continual pre-training on pre-trained LLMs using a text corpus different from the original pre-training dataset. Current post-training approaches for real-world applications involve fine-tuning popular base models (Dubey et al., 2024; Jiang et al., 2023; Rivière et al., 2024) with standard decoder-based architectures that have scaled to hundreds of billions of parameters. However, these approaches face two widely recognized challenges in deploying post-trained models (Xiao et al., 2024; Wang et al., 2024a; He et al., 2024; Brandon et al., 2024; Chen et al., 2024): (1) the substantial memory overhead required for KV-cache storage during inference, and (2) the computational latency, which leads to noticeable inference time.

In the literature, researchers have explored methods to achieve efficient inference and identified significant redundancies *inside and across LLM layers*. This has further led to the development of corresponding efficient architectures: intra-layer Key-Value (KV) sharing, including MQA (Shazeer, 2019) GQA (Ainslie et al., 2023), and cross-layer KV sharing, including CLA (Brandon et al., 2024) and YOCO (Sun et al., 2024). Intra-layer KV sharing methods have been adopted by several open-source base models, including LLaMA-3.1

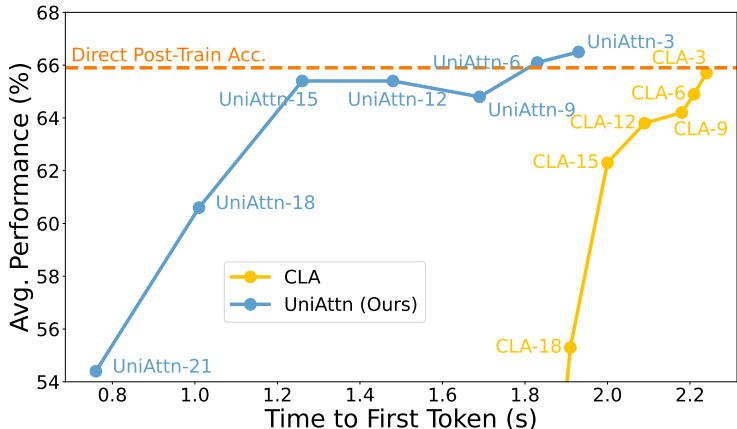


Figure 1: Comparisons of our UniAttn and directly applying cross-layer KV sharing (CLA) during post-training. “A-X” represents modifying total of X layers when applying method A.

(Dubey et al., 2024) and Gemma-2 (Rivière et al., 2024), but these models still incur high inference costs. While cross-layer KV sharing has the potential to further reduce inference costs on top of intra-layer KV sharing methods, directly sharing KV-cache across pre-trained LLM layers results in significant performance degradation (Yang et al., 2024). This raises a critical question: *Which components in pre-trained LLMs are redundant, and how can they be leveraged to reduce inference costs during post-training while maintaining acceptable performance?*

To address this issue, we first conduct a comprehensive analysis of cross-layer KV sharing during post-training. Similar to the training-free scenario (Yang et al., 2024), as shown in Figure 1, cross-layer KV sharing results in substantial performance drops during post-training. To understand this, we then conduct a theoretical analysis and find that cross-layer KV sharing diminishes the impact of model depth on model activations in pre-trained LLMs. Consequently, it undermines the benefits associated with model depth (Wang et al., 2024b), limiting the pre-trained model’s ability to learn new capabilities during post-training. Therefore, alternative approaches beyond cross-layer KV sharing should be explored for post-training.

These findings prompted us to explore other redundancies in pre-trained LLMs, leading to two key observations. First, the Softmax operation significantly contributes to inference costs. Performing the Softmax operation requires access to the entire K-cache. Although the Softmax operation accounts for less than 1% of the FLOPs compared to the linear projections in the backbone, it results in higher latency than the linear projections (Koochpayegani & Pirsivash, 2024). Second, the Softmax operation does not account for the entire impact of model depth on model activations. Unlike cross-layer KV sharing, we demonstrate in Section 3.4 that eliminating the Softmax operation does not diminish the effect of model depth. Motivated by these observations, we further assess the importance of Softmax operations using a similarity-based metric (Men et al., 2024). Our analysis reveals that Softmax activations exhibit high cross-layer similarity in the *top half layers* across various open-source pre-trained LLMs and post-training datasets. This observation suggests a generalizable approach to leveraging Softmax redundancies during post-training.

In this paper, we propose to post-train LLMs with Softmax **Unification in Attention (UniAttn)**. Specifically, we group consecutive transformer blocks in the LLM as several “Superblocks”, and unify the Softmax activations of all blocks within each Superblock. This approach significantly reduces memory and inference costs. Additionally, we observe that the error introduced by unifying Softmax activations can be compensated by a linear projection, and in turn design a pipeline to initialize and train the linear projection. We conduct extensive experiments on 4 open-source pre-trained LLMs across two post-training

scenarios: enhancing domain-specific capabilities and improving general capabilities. Our results demonstrate that UniAttn consistently achieves performance comparable to standard post-training while reducing inference costs. Compared to directly applying existing efficient architectures to post-training, UniAttn achieves substantially better performance with lower inference costs. Furthermore, our UniAttn can be combined with KV-Cache compression methods to further cut down the memory overhead, showing strong practicality for real-world applications.

Overall, we summarize our contribution as follows:

- We consider a critical and practical challenge of leveraging the redundancies in pre-trained LLMs for post-training. We show theoretically and experimentally that existing methods are suboptimal.
- We study the redundancies in pre-trained LLMs and discovered significant redundancies in the Softmax operation. We propose Softmax **Uni**fication in **Attention** (**UniAttn**) for post-training LLMs. Specifically, we unify the Softmax activations across blocks inside the LLM. Additionally, we leverage linear projection to compensate for the error from Softmax unification.
- Extensive experiments show that UniAttn achieves comparable performance to standard post-training while reducing inference costs, and outperforms existing efficient architectures as well.

## 2 Related Works

### 2.1 Post-Training LLMs

Building frontier LLMs for real-world applications involves two crucial stages: pre-training and post-training. Since pre-training data and methodologies are often proprietary, the research community has extensively explored post-training upon open-source pre-trained LLMs (Dubey et al., 2024; Rivière et al., 2024; Jiang et al., 2023) to enhance their *general* or *domain-specific* capabilities for deployment (Lian et al., 2024). Post-training is typically performed on instruction-following or domain-specific datasets. Recently, various datasets have been curated to equip LLMs with specific abilities, including general instruction-following models (Teknum et al., 2024; Lambert et al., 2024; BAAI, 2024), medical QA models (Wu et al., 2023; Gururajan et al., 2024; Singhal et al., 2023), legal QA models (Huang et al., 2023; Zhou et al., 2024), and models with strong mathematical problem-solving capabilities (Liu & Low, 2023).

Existing research on post-training mainly focuses on creating specific datasets for equipping open-source LLMs with specific capabilities. Differently, we investigate the redundancies in pre-trained LLMs and leverage them for post-training inference-efficient LLMs.

### 2.2 Efficient LLM Architectures

Efficient architectures utilize structural redundancies to create inference efficient model variants (Bolya et al., 2023; Xiong et al., 2024) for deployment. In the scope of LLMs, efficient architectures mainly fall into two categories: intra-layer KV sharing, including MQA (Shazeer, 2019) and GQA (Ainslie et al., 2023), and cross-layer KV sharing, including CLA (Brandon et al., 2024) and YOCO (Sun et al., 2024). Specifically, MQA (Shazeer, 2019) simplifies the attention mechanism by utilizing multiple query heads and a single KV head. GQA (Ainslie et al., 2023) takes a step further from MQA by organizing query heads as multiple groups and assigns different KV heads to each group. CLA (Brandon et al., 2024) proposes a cross-layer sharing mechanism to further reduce KV-cache memory overhead by sharing KV-cache across different layers. YOCO (Sun et al., 2024) transforms the original structure into self-decoders and cross-decoders, and adopts a global KV-cache across decoders.

Existing intra-layer KV sharing works have been adopted by various open-source LLMs (Dubey et al., 2024; Jiang et al., 2023; Rivière et al., 2024). However, due to their inherent

massive scale, those models still incur significant inference costs. According to our analysis in Figure 1 and Section 3.2, directly applying cross-layer KV sharing for post-training is suboptimal. To address this, we propose UniAttn, which achieves promising performance for post-training LLMs and outperforms competing methods.

### 3 Methodology

#### 3.1 Preliminaries

In this paper, we focus on mainstream decoder-only LLMs with a transformer structure. Each transformer block in an LLM features a multi-head self-attention (MHA) module and a feed-forward network (FFN). Given an input sequence  $\mathbf{x} \in \mathbb{R}^{l \times d}$  where  $l$  denotes the sequence length and  $d$  denotes the hidden size, both MHA and FFN generate an output sequence with identical length and shape. We focus on the MHA module. Formally, we denote MHA output in layer  $i$  as  $\mathbf{x}'_i$ , where  $\mathbf{x}'_i = \text{MHA}(\text{Norm}(\mathbf{x}_i)) + \mathbf{x}_i$ . "Norm( $\cdot$ )" denotes the Pre-Norm, a component adopted by mainstream open-source LLMs (Dubey et al., 2024; Jiang et al., 2023; Rivière et al., 2024; Bai et al., 2023). In the MHA module, each token in the input sequence  $\mathbf{x}$  is first being projected by  $W_Q$ ,  $W_K$ , and  $W_V$ , forming  $Q, K \in d \times d_k$  and  $V \in d \times d_v$ . Then, the Softmax activation  $s_i$  is calculated by:

$$s = \text{softmax}\left(\frac{QK^T}{\sqrt{d_k}}\right). \quad (1)$$

Subsequently,  $s$  is projected using  $V$  and the weight matrix  $W_o$ , and the input to MHA is added back through a residual connection to produce the MHA output  $\mathbf{x}'_i$ :

$$\mathbf{x}'_i = sVW_o + \mathbf{x}_i \quad (2)$$

#### 3.2 Analysis on Existing Methods

To address redundancies in LLMs, mainstream efficient LLM architectures typically remove insignificant modules in the backbone. Among these methods, intra-layer KV sharing methods such as GQA (Ainslie et al., 2023) has been widely adopted by numerous open-source pre-trained models, like LLaMA3, Mistral, and Gemma2. On the other hand, cross-layer KV sharing methods, including CLA (Brandon et al., 2024) and YOCO (Sun et al., 2024), share the same KV-cache across different layers. Through theoretical analysis, we show that cross-layer KV sharing diminishes the impact of model depth on model activations. This negatively affects the capabilities of pre-trained models, as model depth is a critical factor in determining their overall performance (Wang et al., 2024b).

We first give a series of conclusions as preliminaries.

**Lemma 3.1.**  $f_i : \mathbb{R}^n \rightarrow \mathbb{R}^n$ ,  $i \in \mathbb{N}$  are LINEAR transformations and  $\text{Norm}(\cdot)$  yields a vector with unit Frobenius-norm (denoted as  $\|\cdot\|$ ). Let  $\mathbf{x}_0 \in \mathbb{R}^n$  be the input to the system. Consider an  $L$ -layer Pre-Norm architecture defined by:

$$\mathbf{x}_k = \mathbf{x}_{k-1} + f_k(\text{Norm}(\mathbf{x}_{k-1})), \quad \text{for } k = 1, 2, \dots, L. \quad (3)$$

If the largest singular value in all transformation matrices is bounded by  $\lambda$ , then:

$$\|\mathbf{x}_L\| \leq \|\mathbf{x}_0\| + \lambda L \quad (4)$$

See Appendix for the proof. Lemma 3.1 shows that a Pre-Norm linear system has bounded growth. The norm of output by each layer grows at most linearly with depth  $L$ .

**Proposition 3.2.** Pre-trained decoder-based LLMs exhibit a high linearity score. Formally, let  $A, B \in \mathbb{R}^{n \times d}$  denote the normalized input and output of a decoder block in LLM, respectively,

$$\min_X \|AX - B\| \approx 1 \quad (5)$$

Proposition 3.2 has been validated by (Razzhigaev et al., 2024) on pre-trained LLMs, suggesting that we can approximate each decoder block by a linear transformation with bounded

singular values, thus placing pre-trained LLMs structurally “close” to a linear Pre-Norm system as in Lemma 3.1. In the following discussion, we approximate pre-trained LLMs with an equivalent linear Pre-Norm system and investigate its input and output in each layer.

**Proposition 3.3.** *The input and output of a layer in pre-trained decoder-based LLMs share a high cosine similarity.*

Proposition 3.3 has been validated by (Men et al., 2024) on pre-trained LLMs, indicating that each layer in LLMs predominantly change the *magnitude* of the activation. We leverage the following conclusion for analyzing the change of activation magnitude.

**Proposition 3.4.** *Training Pre-Norm transformers leads to top layers receiving smaller updates (gradient norms decrease from bottom to top).*

(Xiong et al., 2020) has given both a theoretical proof sketch and experimental evidence of Proposition 3.4. Together with Proposition 3.2, we can reasonably assume that the largest singular values of the top layers tend to be smaller after training (See Appendix for demonstration). Since pre-trained LLMs mainly change the magnitude of the activation (as shown in Proposition 3.3), we can use the size of the largest singular values in each layer as an indicator of the corresponding activation magnitude change. This leads to the assumption that the top-layer transformations generally generate outputs with smaller norms.

**Assumption 3.5.** In top layers of **pre-trained** Pre-Norm LLMs:

$$\mathbf{x}_{i+1} = \mathbf{x}_i + \delta, \quad \text{where} \quad \|\delta\| \ll \|\mathbf{x}_i\|. \quad (6)$$

We define  $\delta$  as the “depth factor” that model applies on activations for further discussion.  $\delta$  represents the extent to which model depth influences activations.

**Analysis on Cross-layer KV Sharing:** We adopt Assumption 3.5 to analyze the cross-layer KV sharing architecture, in which KV-cache is shared across multiple consecutive layers. Suppose layer  $i + 1$  shares the KV-cache from layer  $i$ , the MHA operation in layer  $i + 1$  can be written as:

$$\mathbf{x}'_{i+1} = \text{softmax}\left(\frac{QK_i^T}{\sqrt{d_k}}\right)V_iW_o + \mathbf{x}_{i+1}, \quad (7)$$

where  $K_i$  and  $V_i$  are the  $K$  and  $V$  matrices from layer  $i$ . We propose that:

**Proposition 3.6.** *In pre-trained Pre-Norm LLMs, cross-layer KV sharing diminishes the “depth factor”  $\delta$  on activations.*

*Proof.* For simplicity, we suppose  $\mathbf{x}_{i+1}$  is already normalized by the Pre-Norm. We can re-write Equation (7) as:

$$\begin{aligned} \mathbf{x}'_{i+1} &= \text{softmax}\left(\frac{\mathbf{x}_{i+1}W_{q,i+1}K_i^T}{\sqrt{d_k}}\right)V_iW_o + \mathbf{x}_{i+1} \\ &= \text{softmax}\left(\frac{(\mathbf{x}_i + \delta)W_{q,i+1}K_i^T}{\sqrt{d_k}}\right)V_iW_o + \mathbf{x}_{i+1} \\ &= \text{softmax}\left(\frac{\mathbf{x}_iW_{q,i+1}K_i^T}{\sqrt{d_k}} + \frac{\delta W_{q,i+1}K_i^T}{\sqrt{d_k}}\right)V_iW_o + \mathbf{x}_{i+1} \end{aligned} \quad (8)$$

Let  $A_i = \frac{\mathbf{x}_iW_{q,i+1}K_i^T}{\sqrt{d_k}}$ ,  $\hat{\delta} = \frac{\delta W_{q,i+1}K_i^T}{\sqrt{d_k}}$ . By expanding Softmax to the first order:

$$\mathbf{x}'_{i+1} = [\text{softmax}(A_i) + J(A_i)\hat{\delta}]V_iW_o + \mathbf{x}_{i+1} + o(\hat{\delta}^2), \quad (9)$$

where  $J(A_i)$  is the Jacobian of Softmax at  $A_i$ . We ignore the  $o(\hat{\delta}^2)$  remainder. (Xiao et al., 2024) has discovered that the pre-trained LLMs generally exhibit an “attention sink” feature, in which self-attentions heavily attend to the “sink token” at the beginning of a sequence.

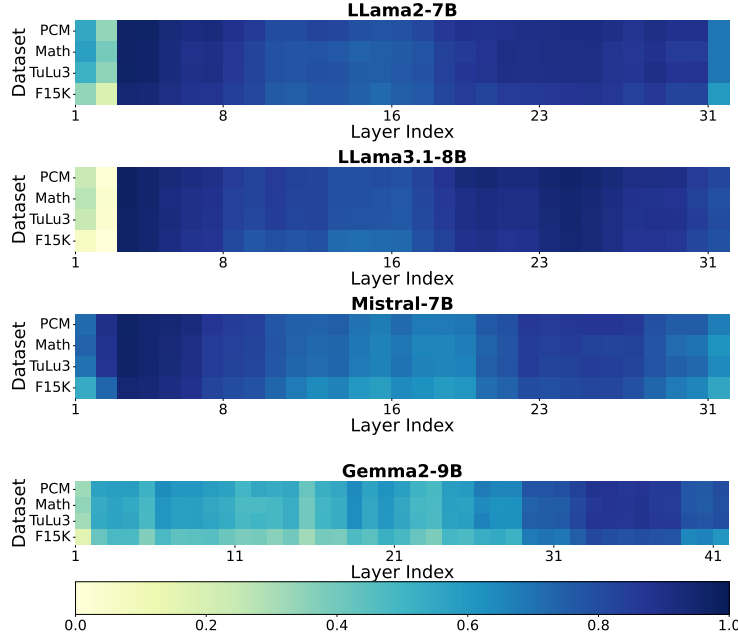


Figure 2: Cosine similarity results of average Softmax activations. Across all settings, the average Softmax activations of the top half of layers share a high cosine similarity very close to 1.

We adopt such feature to estimate  $\|J(A_i)\|$ . According to the statistical pattern concluded by (Xiao et al., 2024), attention logits  $\mathbf{a} \in \mathbb{R}^l$  of a sequence with length  $l$  is approximately:

$$a_i = 1 \ (0 < i < d), \ a_j = -1 \ (i \geq d), \ d \ll l \quad (10)$$

(Xiao et al., 2024) empirically adopts  $d = 4$ . For a sequence of  $l = 1024$ ,  $\|J(\text{softmax}(\mathbf{a}))\| \approx 0.03 \ll 1$ , and decreases as  $l$  increases. Therefore, we can conclude that the coefficient of the  $\delta$  term is significant smaller than that of the Softmax term, making the contribution of the “depth factor” negligible.  $\square$

Proposition 3.6 shows that cross-layer KV sharing diminishes the impact of model depth on model activations. When further analyzing the Softmax term, we derive the following:

$$\begin{aligned} \mathbf{x}'_{i+1} &= \text{softmax}(A_i)V_iW_o + \mathbf{x}_{i+1} \\ &= \text{softmax}\left(\frac{\mathbf{x}_iW_{q,i+1}K_i^T}{\sqrt{d_k}}\right)V_iW_o + \mathbf{x}_{i+1}. \end{aligned} \quad (11)$$

The only difference between the first term in Equation (11) and conducting MHA on  $\mathbf{x}'_i$  is that they use different  $W_q$  matrices. Consequently, the MHA module in layer  $i + 1$  can be interpreted as another query head for the MHA module in layer  $i$ . In essence, *cross-layer KV sharing transforms MHA modules in different layers into additional query heads in a single layer.*

### 3.3 UniAttn: Softmax Unification in Attention

To achieve both memory-efficiency and inference acceleration, we investigate the Softmax operation because (1) calculating Softmax demands the entire K-cache that accounts for 50% memory of the KV-cache; and (2) multiple studies (Geng et al., 2018; Koohpayegani & Pirsivash, 2024) have recognized that the Softmax operation leads to high inference latency. We study the redundancy of Softmax activations in pre-trained LLMs by measuring the importance of Softmax operations in each layer. To ensure the generalizability of our study,



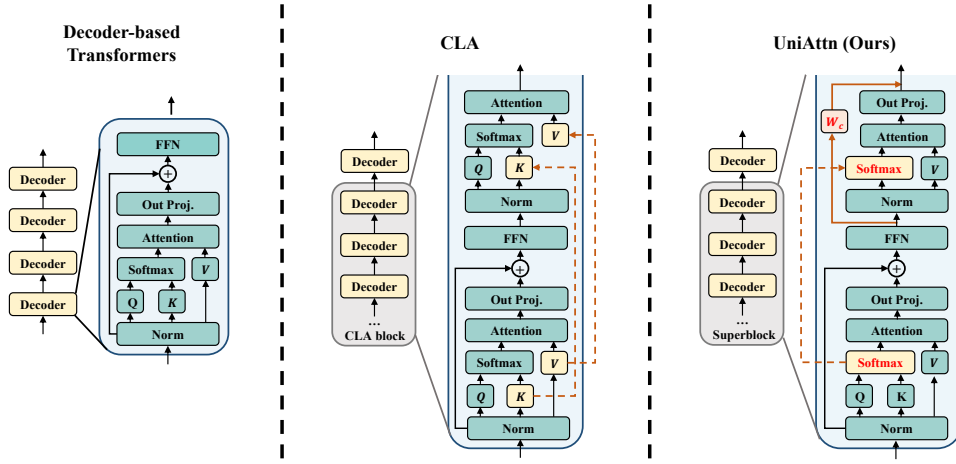


Figure 3: Pipeline comparison between standard decoder-based transformers, CLA (Brandon et al., 2024), and UniAttn. UniAttn shares the Softmax activations across layers in grouped Superblocks and adds linear transformation  $W_c$  to compensate for the unification error.

we employ post-training datasets PMC (Wu et al., 2023), Infinity Instruct (Math) (BAAI, 2024), Tulu3 (Lambert et al., 2024), and long samples (F15K) provided by (Su, 2023), and utilize LLaMA-2 7B (Touvron et al., 2023), LLaMA-3.1 8B (Dubey et al., 2024), Mistral 7B (Jiang et al., 2023), and Gemma-2 9B (Rivière et al., 2024). We collect all Softmax activations, i.e., the  $s$  vectors in Equation (1), and compute the cosine similarity  $\text{Sim}(i) = \cos(s_i, s_{i-1})$  for each sequence. We then average  $\text{Sim}(i)$  over all sequences. As shown in Figure 2, Softmax activations in *top half layers* share a high cross-layer similarity across different experiment settings. This observation shows that Softmax operations are highly redundant in LLMs.

Motivated by such redundancy, we propose **Softmax Unification in Attention (UniAttn)** for post-training LLMs. Specifically, UniAttn groups consecutive decoders in LLMs as “Superblocks”, and unifies the Softmax activations inside each Superblock to reduce the full Softmax operations and KV-cache size during inference. Additionally, we observe that the error introduced by Softmax unification can be compensated by a linear projection, and in turn design a pipeline to initialize and train the linear projection. UniAttn simultaneously reduces the GPU memory and inference latency while achieving competitive performance. Different from cross-layer KV sharing, UniAttn does not diminish the “depth factor”. We show this in Section 3.4.

**Unify Softmax Activations in Superblocks.** To apply UniAttn, we first merge several consecutive transformer blocks as “SuperBlocks”. For simplicity, we create SuperBlocks of the same size. Inside each SuperBlock, only the bottom block employs the Softmax operation. Other blocks simply re-use the Softmax activation matrix  $s$  calculated by the bottom block in the SuperBlock. Formally, for layer  $i + b$  that re-use the Softmax activation  $s_i$  from layer  $i$ :

$$\mathbf{x}'_{i+b} = s_i V_{i+b} W_o + \mathbf{x}_{i+b} \quad (12)$$

Since only the bottom block contribute to calculating the Key projection, other blocks that re-use Softmax activations do not store their corresponding K-cache, leading to GPU memory-efficiency. Moreover, removing Softmax calculations in those layers also contribute to inference latency reduction. Similar to cross-layer KV sharing, UniAttn is also orthogonal to intra-layer KV sharing. In Section 4, we employ pre-trained LLMs with GQA to evaluate UniAttn.

**Linear Compensation.** Simply unifying Softmax activations unavoidably introduces errors in the forward pass. Formally, the error  $\epsilon$  in layer  $i + 1$  is:

$$\begin{aligned}\epsilon &= \mathbf{x}_{i+b}^{\text{ori}'} - \mathbf{x}_{i+b}^{\text{uni}'} \\ &= (\text{softmax}(\frac{Q_{i+b}K_{i+b}^T}{\sqrt{d_k}}) - s_i)V_{i+b}W_o + (\mathbf{x}_{i+b}^{\text{ori}} - \mathbf{x}_{i+b}^{\text{uni}})\end{aligned}\quad (13)$$

where  $\mathbf{x}_{i+b}^{\text{ori}}$  and  $\mathbf{x}_{i+b}^{\text{Uni}}$  denote the input to layer  $i + b$  in the original model and the model with UniAttn applied, respectively. According to (Koochpayegani & Pirsavash, 2024), calculating linear projections yield *significantly lower* latency compared to the Softmax operation. And thus we study the effectiveness of compensating  $\epsilon$  with a linear projection matrix  $W_c$ . To compensate for  $\epsilon$ , we apply  $W_c$  to each layer with unified Softmax activations as:

$$\mathbf{x}'_{i+b} = s_i V_{i+1} W_o + \mathbf{x}_{i+b} + \mathbf{x}_{i+b} W_c \quad (14)$$

We initialize  $W_c$  according to the following Theorem:

**Theorem 3.7.** *The optimal initialization for  $W_c$  satisfies:*

$$W_c = V\Sigma^+U^T\mathbb{E}(\epsilon), \quad (15)$$

where  $U\Sigma V^T$  denotes the SVD decomposition of  $\mathbb{E}(\mathbf{x}_{i+b})$ ,  $\Sigma^+$  denotes the pseudoinverse of  $\Sigma$ .

We leave the proof in the Appendix. In practice, we forward a small portion of training data from the post-training datasets, and use the average values  $\bar{\mathbf{x}}_{i+b}$  and  $\bar{\epsilon}$  as estimations of  $\mathbb{E}(\mathbf{x}_{i+b})$  and  $\mathbb{E}(\epsilon)$ . Considering that compensating for errors in previous layers would influence the calculation in subsequent layers, we calculate the initialization of  $W_c$  bottom-up. Experiments on the F15K dataset (Su, 2023) with sequence length 5,120 yield errors of 11.09 (LLaMA-2 7B) and 5.76 (LLaMA-3.1 8B) after linear compensation, representing only 2.9% and 6.4% of the error before compensation, respectively, well demonstrating its effectiveness. See the appendix for more theoretical insights.

To better train the linear transformations, we adopt a two-stage post-training pipeline. In the first stage, we only fine-tune the  $W_c$  weights and keep other weights frozen. Early stop is also adopted in the first stage. We then conduct a full fine-tuning in the second stage. We formalize a detailed pipeline in Algorithm 1 in the Appendix.

### 3.4 Discussion

Our UniAttn reduces both memory cost and inference latency simultaneously. We underscore that unlike cross-layer KV sharing, our UniAttn does not diminish the “depth factor”  $\delta$  in the forward pass.

**Proposition 3.8.** *In pre-trained Pre-Norm LLMs, the “depth factor” in UniAttn forward pass is unignorable.*

*Proof.* In the forward pass of UniAttn:

$$\begin{aligned}\mathbf{x}'_{i+1} &= s_i(\mathbf{x}_{i+1}W_{v,i+1})W_o + \mathbf{x}_{i+1} \\ &= s_i((\mathbf{x}_i + \delta)W_{v,i+1})W_o + \mathbf{x}_{i+1} \\ &= s_i\mathbf{x}_iW_{v,i+1}W_o + s_i\delta W_{v,i+1}W_o + \mathbf{x}_{i+1}\end{aligned}\quad (16)$$

As  $\mathbf{x}_i$  and  $s_i$  have undergone the same multiplications, we can assume that UniAttn does not modify the relative size of both terms. Since we do not ignore the depth factor  $\delta$ , we consider  $s_i\delta W_{v,i+1}W_o$  is unignorable.  $\square$

## 4 Experiments

### 4.1 Experimental Settings

**Post-Training Settings.** We consider two post-training settings to validate our UniAttn: fine-tuning on domain-specific datasets and on general instruction following datasets. We



Table 1: Post-training performance (%) comparison. **Bold** and underline denote the best and second-best performance of compressed models. For each method, we report their time to first token (TTFT, in seconds) and KV-cache retain rate (KV Cache).

| Method                      | TTFT (s)    | KV Cache | Medical     |             |             |             | General     |               |             |  |
|-----------------------------|-------------|----------|-------------|-------------|-------------|-------------|-------------|---------------|-------------|--|
|                             |             |          | PubMedQa    | MedMCQA     | MedQA       | AVG         | SIQA        | CommonsenseQA | AVG         |  |
| <b>LLama3.1-8B (w/ GQA)</b> |             |          |             |             |             |             |             |               |             |  |
| Pre-Trained                 | 2.26        | 100%     | 75.0        | 56.8        | 59.1        | 63.6        | 46.8        | 71.7          | 59.3        |  |
| Post-Train                  | <u>2.26</u> | 100%     | 75.4        | 59.0        | 63.2        | 65.9        | 50.1        | 73.9          | 62.0        |  |
| LLMDrop-Half                | 1.77        | 81.3%    | 75.6        | <u>57.8</u> | <u>61.5</u> | <u>65.0</u> | 51.4        | <u>75.0</u>   | <u>63.2</u> |  |
| LLMDrop-Full                | <b>1.47</b> | 62.5%    | <u>78.2</u> | 53.6        | 55.9        | 62.6        | <b>51.8</b> | 73.3          | 62.6        |  |
| CLA-Half                    | 2.18        | 81.3%    | 73.8        | <b>58.1</b> | <b>62.8</b> | 64.9        | <u>51.7</u> | 74.7          | <u>63.2</u> |  |
| CLA-Full                    | 2.23        | 62.5%    | 75.4        | 56.9        | 59.2        | 63.8        | <u>50.7</u> | 71.2          | 61.0        |  |
| UniAttn (Ours)              | <u>1.48</u> | 81.3%    | <b>79.0</b> | 57.6        | 59.5        | <b>65.4</b> | 51.1        | <b>75.6</b>   | <b>63.4</b> |  |
| <b>LLama2-7B (w/o GQA)</b>  |             |          |             |             |             |             |             |               |             |  |
| Pre-Trained                 | 2.20        | 100%     | 71.4        | 32.2        | 34.7        | 46.1        | 50.2        | 51.1          | 52.7        |  |
| Post-Train                  | 2.20        | 100%     | 75.4        | 48.8        | 49.2        | 57.8        | 51.6        | 66.3          | 59.0        |  |
| LLMDrop-Half                | 1.74        | 81.3%    | <u>75.2</u> | 48.4        | 49.8        | <u>57.8</u> | <u>51.7</u> | <u>66.7</u>   | <u>59.2</u> |  |
| LLMDrop-Full                | <b>1.37</b> | 62.5%    | 75.0        | <u>48.8</u> | 48.8        | 57.5        | 51.2        | 65.2          | 58.2        |  |
| CLA-Half                    | 2.20        | 81.3%    | 74.4        | 48.4        | <b>50.6</b> | <u>57.8</u> | 51.3        | 66.1          | 58.7        |  |
| CLA-Full                    | 2.23        | 62.5%    | <u>75.2</u> | 45.7        | 47.5        | 56.1        | 50.2        | 65.6          | 57.9        |  |
| UniAttn (Ours)              | <u>1.44</u> | 81.3%    | <b>75.6</b> | <b>49.4</b> | <u>50.1</u> | <b>58.4</b> | <b>51.9</b> | <b>67.7</b>   | <b>59.8</b> |  |

choose PMC (Wu et al., 2023) as the domain-specific dataset and evaluate fine-tuned models on PubMedQA (Jin et al., 2019), MedMCQA (Pal et al., 2022), and MedQA (Jin et al., 2020). We choose Tulu3 (Lambert et al., 2024) as the general instruction following dataset and evaluate fine-tuned models on SIQA (Sap et al., 2019) and CommonsenseQA (Talmor et al., 2019). We employ (Gao et al., 2024) to perform all benchmark evaluations.

**Model.** We post-train 4 open-source pre-trained LLMs for evaluating our UniAttn: LLaMA-2 7B (Touvron et al., 2023), LLaMA-3.1 8B (Dubey et al., 2024), Mistral 7B (Jiang et al., 2023), and Gemma-2 9B (Rivière et al., 2024). We use base models that have undergone only pre-training.

**Implementation details.** We adopt the pattern in Figure 2 and apply UniAttn in the *top half of layers*. Unless otherwise noted, we adopt Superblock size = 4, which yields a total of 4 Superblocks in LLaMA-2 7B, LLaMA-3.1 8B, Mistral 7B, and 5 Superblocks in Gemma-2 9B. For all experiments, we post-train LLMs for 1 epoch. We adopt all training hyperparameter values based on existing research. All training experiments were conducted on 8 H800 GPUs. For time to first token (TTFT) time measurement, we use a single H800 GPU and context length of 8,192 and measure the time to generate the first token after receiving the sequence input. See the Appendix for more details.

## 4.2 Performance Comparison on Post-Training

We verify the effectiveness of UniAttn on 2 open-source LLMs with different architectures, namely LLaMA-3.1 8B (with GQA) (Dubey et al., 2024) and LLaMA-2 7B (without GQA) (Touvron et al., 2023). Please refer to the Appendix for more results on Mistral 7B (Jiang et al., 2023) and Gemma-2 9B (Rivière et al., 2024). We use LLMDrop (He et al., 2024) and CLA (Brandon et al., 2024) as competing efficient architectures, as both methods exploit the cross-layer redundancies in LLMs. For LLMDrop, we bypass the MHA modules with the highest input-output similarities in the top half of the layers. For CLA, we group the top half of the layers into CLA blocks, using the same configuration as in the grouping of Superblocks. Since both competing methods drop the entire KV-cache in the operated layers, we compare two configurations: one with the same operating layers (X-Full) and another with the same KV-cache compression ratio (half operating layers, X-Half). We also conduct post-training after applying these methods.

**Main Conclusion.** We compare different efficient architectures against directly post-training the original LLM (Post-Train) and using the pre-trained model (Pre-Trained) as baselines, as shown in Table 1. Among all competing architectures, our UniAttn achieves the best overall performance across model structures (with and without GQA) and post-training datasets.

Table 2: Ablation study results. **Bold** and underline denote the best and second-best performance of compressed models.

| Method     | Unify Softmax | Compensation | Init $W_c$              | PubMed      | MedMCQA     | MedQA       | AVG         |
|------------|---------------|--------------|-------------------------|-------------|-------------|-------------|-------------|
| Post-Train | -             | -            | -                       | 75.4        | 59.0        | 63.2        | 65.9        |
| UniAttn    | ✓             | ×            | ×                       | 77.0        | 55.7        | <u>58.8</u> | 63.8        |
|            | ✓             | ✓            | zero-init               | 78.0        | 55.8        | 58.1        | 63.9        |
|            | ✓             | ✓            | Theorem 3.7             | <u>78.2</u> | <u>57.1</u> | 58.4        | <u>64.6</u> |
|            | ✓             | ✓            | Theorem 3.7 + fine-tune | <b>79.0</b> | <b>57.6</b> | <b>59.5</b> | <b>65.4</b> |

Table 3: Results of inference cost analysis. “H<sub>2</sub>O Comp.” denotes the compression rate introduced by H<sub>2</sub>O and “KV-Cache” denotes the KV-Cache retain rate.

| Method                   | TTFT (s) | H <sub>2</sub> O Comp. | KV-Cache | AVG  |
|--------------------------|----------|------------------------|----------|------|
| Post-Train               | 2.26     | -                      | 100%     | 65.9 |
| CLA-Half                 | 2.18     | -                      | 81.3%    | 64.9 |
| CLA-Full                 | 2.23     | -                      | 62.5%    | 63.8 |
| UniAttn                  | 1.48     | -                      | 81.3%    | 65.4 |
|                          | 1.48     | 20%                    | 65.0%    | 65.2 |
| UniAttn+H <sub>2</sub> O | 1.46     | 40%                    | 48.8%    | 65.0 |
|                          | 1.46     | 60%                    | 32.5%    | 63.3 |

Besides significantly reducing inference costs in both time and memory, UniAttn maintains comparable performance to directly post-training the original model, well demonstrating its effectiveness. When comparing UniAttn with LLMDrop-Full, we observe that Softmax unification provides a similar acceleration rate to bypassing the entire MHA module, but it achieves significantly better post-training performance. This aligns with our finding that Softmax operations are both costly and redundant. When comparing to CLA, UniAttn achieves better performance with significantly lower inference latency, demonstrating that the UniAttn architecture is better suited for post-training than cross-layer KV sharing.

**Analysis of CLA.** Since CLA only reduces the latency associated with KV projections, its impact on TTFT is minimal. As a result, CLA-Half, CLA-Full, and the original model exhibit comparable TTFT times. Furthermore, CLA achieves comparable performance to LLMDrop when applied to the same number of layers. This suggests that the cross-layer attention mechanism employed by CLA is structurally equivalent to directly bypassing the MHA module. This observation supports our theoretical analysis that cross-layer KV sharing methods like CLA can diminish the depth factor in pre-trained LLMs, in turn limiting their performance.

### 4.3 Experimental Analysis

We choose LLaMA-3.1 8B (Dubey et al., 2024) and the medical domain to conduct experimental analysis. Please refer to the Appendix for more analysis experiments.

**Ablation Studies.** We do controlled experiments to evaluate the impact of each component in UniAttn, namely Softmax unification, linear compensation  $W_c$ , and the initialization for  $W_c$ . The results are shown in Table 2. We observe that after unifying the Softmax activations, both adding linear compensation and using proper initialization contribute positively to the final performance. While linear compensation consistently improves performance across different initialization methods, appropriate initialization proves critical for effectively fine-tuning  $W_c$ .

**Inference Cost Analysis.** We evaluate and compare inference costs to demonstrate the efficiency of UniAttn. To further maximize its potential, we integrate UniAttn with the KV-Cache compression method H<sub>2</sub>O (Zhang et al., 2023) to further reduce memory overhead by keeping only the essential and the recent tokens in the KV-cache. We report the TTFT latency and the total KV-cache retain rate. As shown in Table 3, UniAttn achieves a significant reduction in TTFT latency compared to CLA under the same KV-cache retain rate. When

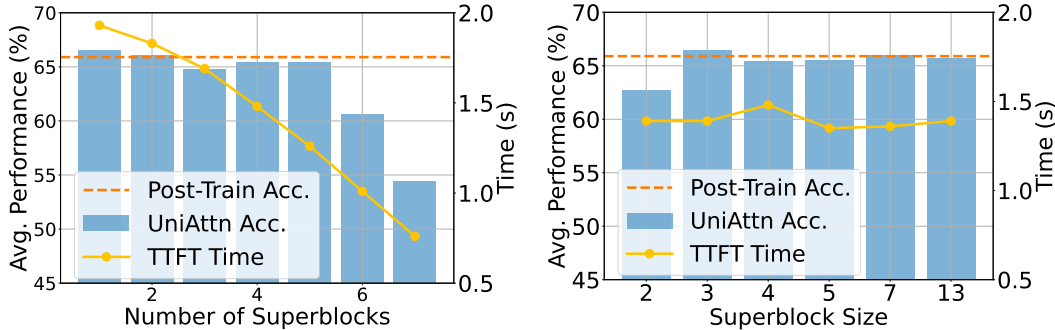


Figure 4: Hyperparameter analysis results (%). Left: The relationship of average accuracy and TTFT latency to the total number of grouped Superblocks (each with size 4). Right: The relationship of average accuracy and TTFT latency to the size of each Superblock (total of 12 layers that utilize unified Softmax activation).

combined with H<sub>2</sub>O, UniAttn+H<sub>2</sub>O reduces the KV-cache retain rate to below 50% while maintaining an average performance of 65.0%, achieving both better performance, lower inference latency, and higher KV-cache compression rate than CLA. These results clearly demonstrate the inference efficiency of UniAttn, highlighting its substantial benefits for real-world deployment scenarios.

**Hyperparameter Analysis.** We perform a hyperparameter analysis on the number and the size of Superblocks to evaluate their impact on latency and post-training performance. First, we examine the effect of varying the number of Superblocks. Using a consistent Superblock size of 4, we group different numbers of Superblocks from the top layers to the bottom layers. For instance, grouping 2 Superblocks indicates that layer 25-28 and 29-32 form the two Superblocks. The results are shown in Figure 4 (left). From the perspective of TTFT latency, increasing the number of Superblocks significantly reduces latency. From the perspective of performance, while grouping certain top layers as Superblocks does not substantially affect model performance, continuing to increase the number of Superblocks leads to sharp performance drops. Second, we analyze the impact of Superblock size. For fair comparison, we maintain a consistent total number of layers that utilize unified Softmax activations from preceding layers as 12. Since a Superblock with size  $b$  unifies Softmax in  $b - 1$  layers, we set  $b$  such that  $b - 1$  is a factor of 12, resulting in Superblock sizes of 2, 3, 4, 5, 7, and 13, and number of Superblocks as 12, 6, 4, 3, 2, and 1, respectively. As shown in Figure 4 (right), the size of the Superblocks does not significantly affect post-training performance. For simplicity, we use a Superblock size of 4, although fine-grained tuning of Superblock size could further improve post-training performance.

## 5 Conclusion

In this work, we explored LLM redundancies and efficient architectures in the context of post-training to reduce the inference costs of LLMs. Theoretically, we identified that the existing cross-layer KV sharing architecture diminishes the depth factor in pre-trained LLMs, potentially limiting their ability to acquire new capabilities during post-training. To address this limitation, we investigated the primary bottleneck in LLMs—the Softmax operation—and discovered significant redundancies across various pre-trained LLMs and datasets. Based on these findings, we proposed UniAttn, an efficient architecture that leverages these redundancies while preserving LLM capabilities through linear compensation in post-training. Extensive experiments on diverse pre-trained models and post-training datasets validate the effectiveness of UniAttn. Our UniAttn is particularly well-suited for real-world deployments, enjoying faster inference and less memory cost.

## References

- Joshua Ainslie, James Lee-Thorp, Michiel de Jong, Yury Zemlyanskiy, Federico Lebrón, and Sumit Sanghai. GQA: training generalized multi-query transformer models from multi-head checkpoints. In Houda Bouamor, Juan Pino, and Kalika Bali (eds.), *Proceedings of the 2023 Conference on Empirical Methods in Natural Language Processing, EMNLP 2023, Singapore, December 6-10, 2023*, pp. 4895–4901. Association for Computational Linguistics, 2023. doi: 10.18653/V1/2023.EMNLP-MAIN.298. URL <https://doi.org/10.18653/v1/2023.emnlp-main.298>.
- BAAI. Infinity instruct, 2024. URL <https://github.com/FlagOpen/Infinity-Instruct>.
- Jinze Bai, Shuai Bai, Yunfei Chu, Zeyu Cui, Kai Dang, Xiaodong Deng, Yang Fan, Wenbin Ge, Yu Han, Fei Huang, et al. Qwen technical report. *arXiv preprint arXiv:2309.16609*, 2023.
- Daniel Bolya, Cheng-Yang Fu, Xiaoliang Dai, Peizhao Zhang, Christoph Feichtenhofer, and Judy Hoffman. Token merging: Your vit but faster. In *The Eleventh International Conference on Learning Representations, ICLR 2023, Kigali, Rwanda, May 1-5, 2023*. OpenReview.net, 2023. URL <https://openreview.net/forum?id=JroZRrW7Eu>.
- William Brandon, Mayank Mishra, Aniruddha Nrusimha, Rameswar Panda, and Jonathan Ragan-Kelley. Reducing transformer key-value cache size with cross-layer attention. *CoRR*, abs/2405.12981, 2024. doi: 10.48550/ARXIV.2405.12981. URL <https://doi.org/10.48550/arXiv.2405.12981>.
- Liang Chen, Haozhe Zhao, Tianyu Liu, Shuai Bai, Junyang Lin, Chang Zhou, and Baobao Chang. An image is worth 1/2 tokens after layer 2: Plug-and-play inference acceleration for large vision-language models. In Ales Leonardis, Elisa Ricci, Stefan Roth, Olga Russakovsky, Torsten Sattler, and Gül Varol (eds.), *Computer Vision - ECCV 2024 - 18th European Conference, Milan, Italy, September 29-October 4, 2024, Proceedings, Part LXXXI*, volume 15139 of *Lecture Notes in Computer Science*, pp. 19–35. Springer, 2024. doi: 10.1007/978-3-031-73004-7\_2. URL [https://doi.org/10.1007/978-3-031-73004-7\\_2](https://doi.org/10.1007/978-3-031-73004-7_2).
- Abhimanyu Dubey, Abhinav Jauhri, Abhinav Pandey, Abhishek Kadian, Ahmad Al-Dahle, Aiesha Letman, Akhil Mathur, Alan Schelten, Amy Yang, Angela Fan, Anirudh Goyal, Anthony Hartshorn, Aobo Yang, Archi Mitra, Archie Sravankumar, Artem Korenev, Arthur Hinsvark, Arun Rao, Aston Zhang, Aurélien Rodriguez, Austen Gregerson, Ava Spataru, Baptiste Rozière, Bethany Biron, Binh Tang, Bobbie Chern, Charlotte Caucheteux, Chaya Nayak, Chloe Bi, Chris Marra, Chris McConnell, Christian Keller, Christophe Touret, Chunyang Wu, Corinne Wong, Cristian Canton Ferrer, Cyrus Nikolaidis, Damien Allonsius, Daniel Song, Danielle Pintz, Danny Livshits, David Esiobu, Dhruv Choudhary, Dhruv Mahajan, Diego Garcia-Olano, Diego Perino, Dieuwke Hupkes, Egor Lakomkin, Ehab AlBadawy, Elina Lobanova, Emily Dinan, Eric Michael Smith, Filip Radenovic, Frank Zhang, Gabriel Synnaeve, Gabrielle Lee, Georgia Lewis Anderson, Graeme Nail, Grégoire Mialon, Guan Pang, Guillem Cucurell, Hailey Nguyen, Hannah Korevaar, Hu Xu, Hugo Touvron, Iliyan Zarov, Imanol Arrieta Ibarra, Isabel M. Kloumann, Ishan Misra, Ivan Evtimov, Jade Copet, Jaewon Lee, Jan Geffert, Jana Vranes, Jason Park, Jay Mahadeokar, Jeet Shah, Jelmer van der Linde, Jennifer Billock, Jenny Hong, Jenya Lee, Jeremy Fu, Jianfeng Chi, Jianyu Huang, Jiawen Liu, Jie Wang, Jiecao Yu, Joanna Bitton, Joe Spisak, Jongsoo Park, Joseph Rocca, Joshua Johnstun, Joshua Saxe, Junteng Jia, Kalyan Vasuden Alwala, Kartikeya Upasani, Kate Plawiak, Ke Li, Kenneth Heafield, Kevin Stone, and et al. The llama 3 herd of models. *CoRR*, abs/2407.21783, 2024. doi: 10.48550/ARXIV.2407.21783. URL <https://doi.org/10.48550/arXiv.2407.21783>.
- Leo Gao, Jonathan Tow, Baber Abbasi, Stella Biderman, Sid Black, Anthony DiPofi, Charles Foster, Laurence Golding, Jeffrey Hsu, Alain Le Noac’h, Haonan Li, Kyle McDonell, Niklas Muennighoff, Chris Ociepa, Jason Phang, Laria Reynolds, Hailey Schoelkopf, Aviya Skowron, Lintang Sutawika, Eric Tang, Anish Thite, Ben Wang, Kevin Wang, and Andy Zou. A framework for few-shot language model evaluation, 07 2024. URL <https://zenodo.org/records/12608602>.

- Xue Geng, Jie Lin, Bin Zhao, Anmin Kong, Mohamed M. Sabry Aly, and Vijay Chandrasekhar. Hardware-aware softmax approximation for deep neural networks. In C. V. Jawahar, Hongdong Li, Greg Mori, and Konrad Schindler (eds.), *Computer Vision - ACCV 2018 - 14th Asian Conference on Computer Vision, Perth, Australia, December 2-6, 2018, Revised Selected Papers, Part IV*, volume 11364 of *Lecture Notes in Computer Science*, pp. 107–122. Springer, 2018. doi: 10.1007/978-3-030-20870-7\\_7. URL [https://doi.org/10.1007/978-3-030-20870-7\\_7](https://doi.org/10.1007/978-3-030-20870-7_7).
- Ashwin Kumar Gururajan, Enrique Lopez-Cuena, Jordi Bayarri-Planas, Adrian Tormos, Daniel Hinjos, Pablo Bernabeu-Perez, Anna Arias-Duart, Pablo Agustin Martin-Torres, Lucia Urcelay-Ganzabal, Marta Gonzalez-Mallo, Sergio Alvarez-Napagao, Eduard Ayguadé-Parra, and Ulises Cortés Dario Garcia-Gasulla. Aloe: A family of fine-tuned open healthcare llms, 2024. URL <https://arxiv.org/abs/2405.01886>.
- Shwai He, Guoheng Sun, Zheyu Shen, and Ang Li. What matters in transformers? not all attention is needed. *CoRR*, abs/2406.15786, 2024. doi: 10.48550/ARXIV.2406.15786. URL <https://doi.org/10.48550/arXiv.2406.15786>.
- Quzhe Huang, Mingxu Tao, Chen Zhang, Zhenwei An, Cong Jiang, Zhibin Chen, Zirui Wu, and Yansong Feng. Lawyer llama technical report, 2023. URL <https://arxiv.org/abs/2305.15062>.
- Albert Q. Jiang, Alexandre Sablayrolles, Arthur Mensch, Chris Bamford, Devendra Singh Chaplot, Diego de Las Casas, Florian Bressand, Gianna Lengyel, Guillaume Lample, Lucile Saulnier, Léo Renard Lavaud, Marie-Anne Lachaux, Pierre Stock, Teven Le Scao, Thibaut Lavril, Thomas Wang, Timothée Lacroix, and William El Sayed. Mistral 7b. *CoRR*, abs/2310.06825, 2023. doi: 10.48550/ARXIV.2310.06825. URL <https://doi.org/10.48550/arXiv.2310.06825>.
- Di Jin, Eileen Pan, Nassim Oufattole, Wei-Hung Weng, Hanyi Fang, and Peter Szolovits. What disease does this patient have? A large-scale open domain question answering dataset from medical exams. *CoRR*, abs/2009.13081, 2020. URL <https://arxiv.org/abs/2009.13081>.
- Qiao Jin, Bhuwan Dhingra, Zhengping Liu, William W. Cohen, and Xinghua Lu. Pubmedqa: A dataset for biomedical research question answering. In Kentaro Inui, Jing Jiang, Vincent Ng, and Xiaojun Wan (eds.), *Proceedings of the 2019 Conference on Empirical Methods in Natural Language Processing and the 9th International Joint Conference on Natural Language Processing, EMNLP-IJCNLP 2019, Hong Kong, China, November 3-7, 2019*, pp. 2567–2577. Association for Computational Linguistics, 2019. doi: 10.18653/V1/D19-1259. URL <https://doi.org/10.18653/v1/D19-1259>.
- Soroush Abbasi Koohpayegani and Hamed Pirsiavash. Sima: Simple softmax-free attention for vision transformers. In *IEEE/CVF Winter Conference on Applications of Computer Vision, WACV 2024, Waikoloa, HI, USA, January 3-8, 2024*, pp. 2595–2605. IEEE, 2024. doi: 10.1109/WACV57701.2024.00259. URL <https://doi.org/10.1109/WACV57701.2024.00259>.
- Nathan Lambert, Jacob Morrison, Valentina Pyatkin, Shengyi Huang, Hamish Ivison, Faeze Brahman, Lester James V. Miranda, Alisa Liu, Nouha Dziri, Shane Lyu, Yuling Gu, Saumya Malik, Victoria Graf, Jena D. Hwang, Jiangjiang Yang, Ronan Le Bras, Oyvind Tafjord, Chris Wilhelm, Luca Soldaini, Noah A. Smith, Yizhong Wang, Pradeep Dasigi, and Hannaneh Hajishirzi. Tulu 3: Pushing frontiers in open language model post-training. *CoRR*, abs/2411.15124, 2024. doi: 10.48550/ARXIV.2411.15124. URL <https://doi.org/10.48550/arXiv.2411.15124>.
- Haoran Lian, Junmin Chen, Wei Huang, Yizhe Xiong, Wenping Hu, Guiguang Ding, Hui Chen, Jianwei Niu, Zijia Lin, Fuzheng Zhang, and Di Zhang. Breaking the stage barrier: A novel single-stage approach to long context extension for large language models, 2024. URL <https://arxiv.org/abs/2412.07171>.
- Haotian Liu, Chunyuan Li, Qingyang Wu, and Yong Jae Lee. Visual instruction tuning. In Alice Oh, Tristan Naumann, Amir Globerson, Kate Saenko, Moritz Hardt, and Sergey



- Levine (eds.), *Advances in Neural Information Processing Systems 36: Annual Conference on Neural Information Processing Systems 2023, NeurIPS 2023, New Orleans, LA, USA, December 10 - 16, 2023*, 2023. URL [http://papers.nips.cc/paper\\_files/paper/2023/hash/6dcf277ea32ce3288914faf369fe6de0-Abstract-Conference.html](http://papers.nips.cc/paper_files/paper/2023/hash/6dcf277ea32ce3288914faf369fe6de0-Abstract-Conference.html).
- Tiedong Liu and Bryan Kian Hsiang Low. Goat: Fine-tuned llama outperforms gpt-4 on arithmetic tasks, 2023. URL <https://arxiv.org/abs/2305.14201>.
- Xin Men, Mingyu Xu, Qingyu Zhang, Bingning Wang, Hongyu Lin, Yaojie Lu, Xianpei Han, and Weipeng Chen. Shortgpt: Layers in large language models are more redundant than you expect. *CoRR*, abs/2403.03853, 2024. doi: 10.48550/ARXIV.2403.03853. URL <https://doi.org/10.48550/arXiv.2403.03853>.
- OpenAI. GPT-4 technical report. *CoRR*, abs/2303.08774, 2023. doi: 10.48550/ARXIV.2303.08774. URL <https://doi.org/10.48550/arXiv.2303.08774>.
- Ankit Pal, Logesh Kumar Umaphathi, and Malaikannan Sankarasubbu. Medmcqa: A large-scale multi-subject multi-choice dataset for medical domain question answering. In Gerardo Flores, George H. Chen, Tom J. Pollard, Joyce C. Ho, and Tristan Naumann (eds.), *Conference on Health, Inference, and Learning, CHIL 2022, 7-8 April 2022, Virtual Event*, volume 174 of *Proceedings of Machine Learning Research*, pp. 248–260. PMLR, 2022. URL <https://proceedings.mlr.press/v174/pal22a.html>.
- Anton Razzhigaev, Matvey Mikhalchuk, Elizaveta Goncharova, Nikolai Gerasimenko, Ivan Oseledets, Denis Dimitrov, and Andrey Kuznetsov. Your transformer is secretly linear. In Lun-Wei Ku, Andre Martins, and Vivek Srikumar (eds.), *Proceedings of the 62nd Annual Meeting of the Association for Computational Linguistics (Volume 1: Long Papers)*, pp. 5376–5384, Bangkok, Thailand, August 2024. Association for Computational Linguistics. doi: 10.18653/v1/2024.acl-long.293. URL <https://aclanthology.org/2024.acl-long.293/>.
- Morgane Rivi re, Shreya Pathak, Pier Giuseppe Sessa, Cassidy Hardin, Surya Bhupatiraju, L onard Hussenot, Thomas Mesnard, Bobak Shahriari, Alexandre Ram , Johan Ferret, Peter Liu, Pouya Tafti, Abe Friesen, Michelle Casbon, Sabela Ramos, Ravin Kumar, Charline Le Lan, Sammy Jerome, Anton Tsitsulin, Nino Vieillard, Piotr Stanczyk, Sertan Girgin, Nikola Momchev, Matt Hoffman, Shantanu Thakoor, Jean-Bastien Grill, Behnam Neyshabur, Olivier Bachem, Alanna Walton, Aliaksei Severyn, Alicia Parrish, Aliya Ahmad, Allen Hutchison, Alvin Abdagic, Amanda Carl, Amy Shen, Andy Brock, Andy Coenen, Anthony Laforge, Antonia Paterson, Ben Bastian, Bilal Piot, Bo Wu, Brandon Royal, Charlie Chen, Chintu Kumar, Chris Perry, Chris Welty, Christopher A. Choquette-Choo, Danila Sinopalnikov, David Weinberger, Dimple Vijaykumar, Dominika Rogozinska, Dustin Herbison, Elisa Bandy, Emma Wang, Eric Noland, Erica Moreira, Evan Senter, Evgenii Eltyshev, Francesco Visin, Gabriel Rasskin, Gary Wei, Glenn Cameron, Gus Martins, Hadi Hashemi, Hanna Klimczak-Plucinska, Harleen Batra, Harsh Dhand, Ivan Nardini, Jacinda Mein, Jack Zhou, James Svensson, Jeff Stanway, Jetha Chan, Jin Peng Zhou, Joana Carrasqueira, Joana Iljazi, Jocelyn Becker, Joe Fernandez, Joost van Amersfoort, Josh Gordon, Josh Lipschultz, Josh Newlan, Ju-yeong Ji, Kareem Mohamed, Kartikeya Badola, Kat Black, Katie Millican, Keelin McDonell, Kelvin Nguyen, Kiranbir Sodhia, Kish Greene, Lars Lowe Sj sund, Lauren Usui, Laurent Sifre, Lena Heuermann, Leticia Lago, and Lilly McNealus. Gemma 2: Improving open language models at a practical size. *CoRR*, abs/2408.00118, 2024. doi: 10.48550/ARXIV.2408.00118. URL <https://doi.org/10.48550/arXiv.2408.00118>.
- Maarten Sap, Hannah Rashkin, Derek Chen, Ronan Le Bras, and Yejin Choi. Socialiqa: Commonsense reasoning about social interactions. *CoRR*, abs/1904.09728, 2019. URL <http://arxiv.org/abs/1904.09728>.
- Zhihong Shao, Peiyi Wang, Qihao Zhu, Runxin Xu, Junxiao Song, Mingchuan Zhang, Y. K. Li, Y. Wu, and Daya Guo. Deepseekmath: Pushing the limits of mathematical reasoning in open language models. *CoRR*, abs/2402.03300, 2024. doi: 10.48550/ARXIV.2402.03300. URL <https://doi.org/10.48550/arXiv.2402.03300>.



- Noam Shazeer. Fast transformer decoding: One write-head is all you need, 2019. URL <https://arxiv.org/abs/1911.02150>.
- Karan Singhal, Tao Tu, Juraj Gottweis, Rory Sayres, Ellery Wulczyn, Le Hou, Kevin Clark, Stephen Pfohl, Heather Cole-Lewis, Darlene Neal, Mike Schaeckermann, Amy Wang, Mohamed Amin, Sami Lachgar, Philip Mansfield, Sushant Prakash, Bradley Green, Ewa Dominowska, Blaise Aguera y Arcas, Nenad Tomasev, Yun Liu, Renee Wong, Christopher Semturs, S. Sara Mahdavi, Joelle Barral, Dale Webster, Greg S. Corrado, Yossi Matias, Shekoofeh Azizi, Alan Karthikesalingam, and Vivek Natarajan. Towards expert-level medical question answering with large language models, 2023. URL <https://arxiv.org/abs/2305.09617>.
- Jianlin Su. Rectified rotary position embeddings. <https://github.com/bojone/rerope>, 2023.
- Yutao Sun, Li Dong, Yi Zhu, Shaohan Huang, Wenhui Wang, Shuming Ma, Quanlu Zhang, Jianyong Wang, and Furu Wei. You only cache once: Decoder-decoder architectures for language models. *CoRR*, abs/2405.05254, 2024. doi: 10.48550/ARXIV.2405.05254. URL <https://doi.org/10.48550/arXiv.2405.05254>.
- Alon Talmor, Jonathan Herzig, Nicholas Lourie, and Jonathan Berant. Commonsenseqa: A question answering challenge targeting commonsense knowledge. In Jill Burstein, Christy Doran, and Thamar Solorio (eds.), *Proceedings of the 2019 Conference of the North American Chapter of the Association for Computational Linguistics: Human Language Technologies, NAACL-HLT 2019, Minneapolis, MN, USA, June 2-7, 2019, Volume 1 (Long and Short Papers)*, pp. 4149–4158. Association for Computational Linguistics, 2019. doi: 10.18653/V1/N19-1421. URL <https://doi.org/10.18653/v1/n19-1421>.
- Ryan Teknium, Jeffrey Quesnelle, and Chen Guang. Hermes 3 technical report, 2024. URL <https://arxiv.org/abs/2408.11857>.
- Arun James Thirunavukarasu, Darren Shu Jeng Ting, Kabilan Elangovan, Laura Gutierrez, Ting Fang Tan, and Daniel Shu Wei Ting. Large language models in medicine. *Nature medicine*, 29(8):1930–1940, 2023.
- Hugo Touvron, Louis Martin, Kevin Stone, Peter Albert, Amjad Almahairi, Yasmine Babaei, Nikolay Bashlykov, Soumya Batra, Prajjwal Bhargava, Shrutu Bhosale, et al. Llama 2: Open foundation and fine-tuned chat models. *arXiv preprint arXiv:2307.09288*, 2023.
- Ao Wang, Hui Chen, Jianchao Tan, Kefeng Zhang, Xunliang Cai, Zijia Lin, Jungong Han, and Guiguang Ding. Prefixkv: Adaptive prefix kv cache is what vision instruction-following models need for efficient generation, 2024a. URL <https://arxiv.org/abs/2412.03409>.
- Hongyu Wang, Shuming Ma, Li Dong, Shaohan Huang, Dongdong Zhang, and Furu Wei. Deepnet: Scaling transformers to 1,000 layers. *IEEE Trans. Pattern Anal. Mach. Intell.*, 46(10):6761–6774, 2024b. doi: 10.1109/TPAMI.2024.3386927. URL <https://doi.org/10.1109/TPAMI.2024.3386927>.
- Chaoyi Wu, Xiaoman Zhang, Ya Zhang, Yanfeng Wang, and Weidi Xie. Pmc-llama: Further finetuning llama on medical papers. *CoRR*, abs/2304.14454, 2023. doi: 10.48550/ARXIV.2304.14454. URL <https://doi.org/10.48550/arXiv.2304.14454>.
- Guangxuan Xiao, Yuandong Tian, Beidi Chen, Song Han, and Mike Lewis. Efficient streaming language models with attention sinks. In *The Twelfth International Conference on Learning Representations, ICLR 2024, Vienna, Austria, May 7-11, 2024*. OpenReview.net, 2024. URL <https://openreview.net/forum?id=NG7sS51zVF>.
- Ruibin Xiong, Yunchang Yang, Di He, Kai Zheng, Shuxin Zheng, Chen Xing, Huishuai Zhang, Yanyan Lan, Liwei Wang, and Tie-Yan Liu. On layer normalization in the transformer architecture. In *Proceedings of the 37th International Conference on Machine Learning, ICML 2020, 13-18 July 2020, Virtual Event*, volume 119 of *Proceedings of Machine Learning Research*, pp. 10524–10533. PMLR, 2020. URL <http://proceedings.mlr.press/v119/xiong20b.html>.

- Yizhe Xiong, Hui Chen, Tianxiang Hao, Zijia Lin, Jungong Han, Yuesong Zhang, Guoxin Wang, Yongjun Bao, and Guiguang Ding. PYRA: parallel yielding re-activation for training-inference efficient task adaptation. In Ales Leonardis, Elisa Ricci, Stefan Roth, Olga Russakovsky, Torsten Sattler, and Gül Varol (eds.), *Computer Vision - ECCV 2024 - 18th European Conference, Milan, Italy, September 29-October 4, 2024, Proceedings, Part IX*, volume 15067 of *Lecture Notes in Computer Science*, pp. 455–473. Springer, 2024. doi: 10.1007/978-3-031-72673-6\_25. URL [https://doi.org/10.1007/978-3-031-72673-6\\_25](https://doi.org/10.1007/978-3-031-72673-6_25).
- Yifei Yang, Zouying Cao, Qiguang Chen, Libo Qin, Dongjie Yang, Hai Zhao, and Zhi Chen. Kvsharer: Efficient inference via layer-wise dissimilar kv cache sharing. *arXiv preprint arXiv:2410.18517*, 2024.
- Zhenyu Zhang, Ying Sheng, Tianyi Zhou, Tianlong Chen, Lianmin Zheng, Ruisi Cai, Zhao Song, Yuandong Tian, Christopher Ré, Clark W. Barrett, Zhangyang Wang, and Beidi Chen. H2O: heavy-hitter oracle for efficient generative inference of large language models. In Alice Oh, Tristan Naumann, Amir Globerson, Kate Saenko, Moritz Hardt, and Sergey Levine (eds.), *Advances in Neural Information Processing Systems 36: Annual Conference on Neural Information Processing Systems 2023, NeurIPS 2023, New Orleans, LA, USA, December 10 - 16, 2023*, 2023. URL [http://papers.nips.cc/paper\\_files/paper/2023/hash/6ceefa7b15572587b78ecfceb2827f8-Abstract-Conference.html](http://papers.nips.cc/paper_files/paper/2023/hash/6ceefa7b15572587b78ecfceb2827f8-Abstract-Conference.html).
- Zhi Zhou, Jiang-Xin Shi, Peng-Xiao Song, Xiao-Wen Yang, Yi-Xuan Jin, Lan-Zhe Guo, and Yu-Feng Li. Lawgpt: A chinese legal knowledge-enhanced large language model, 2024. URL <https://arxiv.org/abs/2406.04614>.

Table 4: Training hyperparameter details of UniAttn.

| Method  | Model        | Learning Rate | Weight Decay | Batch Size | Epochs | Superblock Size | Superblock Groups                           |
|---------|--------------|---------------|--------------|------------|--------|-----------------|---|
| UniAttn | LLaMA-2 7B   | 2e-5          | 0            | 48         | 1      | 4               | [17-20], [21-24], [25-28], [29-32]          |
|         | LLaMA-3.1 8B | 7e-6          | 0            | 48         | 1      | 4               | [17-20], [21-24], [25-28], [29-32]          |
|         | Mistral 7B   | 1e-6          | 0            | 48         | 1      | 4               | [17-20], [21-24], [25-28], [29-32]          |
|         | Gemma-2 9B   | 1e-6          | 0            | 48         | 1      | 4               | [22-25], [26-29], [30-33], [34-37], [38-41] |

Table 5: Training hyperparameter details of CLA.

| Method   | Model        | Learning Rate | Weight Decay | Batch Size | Epochs | CLA Block Size | CLA Block Groups                            |
|----------|--------------|---------------|--------------|------------|--------|----------------|---|
| CLA-Half | LLaMA-2 7B   | 2e-5          | 0            | 48         | 1      | 4              | [25-28], [29-32]                            |
|          | LLaMA-3.1 8B | 7e-6          | 0            | 48         | 1      | 4              | [25-28], [29-32]                            |
|          | Mistral 7B   | 1e-6          | 0            | 48         | 1      | 4              | [25-28], [29-32]                            |
|          | Gemma-2 9B   | 1e-6          | 0            | 48         | 1      | 4              | [30-33], [34-37], [38-41]                   |
| CLA-Full | LLaMA-2 7B   | 2e-5          | 0            | 48         | 1      | 4              | [17-20], [21-24], [25-28], [29-32]          |
|          | LLaMA-3.1 8B | 7e-6          | 0            | 48         | 1      | 4              | [17-20], [21-24], [25-28], [29-32]          |
|          | Mistral 7B   | 1e-6          | 0            | 48         | 1      | 4              | [17-20], [21-24], [25-28], [29-32]          |
|          | Gemma-2 9B   | 1e-6          | 0            | 48         | 1      | 4              | [22-25], [26-29], [30-33], [34-37], [38-41] |

Table 6: Training hyperparameter details of LLMDrop. The index of dropped layers are ordered by input-output similarity.

| Method       | Model        | Learning Rate | Weight Decay | Batch Size | Epochs | # of Dropped Layers | Index of Dropped Layers                      |
|--------------|--------------|---------------|--------------|------------|--------|---------------------|--|
| LLMDrop-Half | LLaMA-2 7B   | 2e-5          | 0            | 48         | 1      | 6                   | 23,20,32,27,22,24                            |
|              | LLaMA-3.1 8B | 7e-6          | 0            | 48         | 1      | 6                   | 19,22,20,21,27,23                            |
|              | Mistral 7B   | 1e-6          | 0            | 48         | 1      | 6                   | 17,32,31,21,22,24                            |
|              | Gemma-2 9B   | 1e-6          | 0            | 48         | 1      | 8                   | 29,26,21,30,27,40,38,31                      |
| LLMDrop-Full | LLaMA-2 7B   | 2e-5          | 0            | 48         | 1      | 12                  | 23,20,32,27,22,24,31,29,25,30,28,26          |
|              | LLaMA-3.1 8B | 7e-6          | 0            | 48         | 1      | 12                  | 19,22,20,21,27,23,30,29,28,26,24,25          |
|              | Mistral 7B   | 1e-6          | 0            | 48         | 1      | 12                  | 17,32,31,21,22,24,29,23,28,25,27,26          |
|              | Gemma-2 9B   | 1e-6          | 0            | 48         | 1      | 15                  | 29,26,21,30,27,40,38,31,32,33,35,39,36,37,34 |

## A More Implementation Details for Reproducibility

**Post-Training Datasets.** Regarding the medical domain, we directly employ the instruction tuning dataset for PMC<sup>1</sup> (Wu et al., 2023) (i.e., training stage-2 for PMC-LLaMA) for post-training. The dataset consists of 513,999 instruction-input-output pairs. Regarding the general instruction tuning scenario, we employ the Tulu 3 SFT Mixture<sup>2</sup> and filter for data with only 1 round of conversation, resulting in 896,070 input-output pairs.

**Training Hyperparameters.** The training hyperparameters for all experiments are reported in Table 4, Table 5, and Table 6. Note that we adopt the learning rate and weight decay values according to existing research, in which those pre-trained models are post-trained under reported schedules.

**Evaluation Details.** For all experiments, we evaluate the final checkpoint after post-training for benchmark evaluation. Regarding the medical domain, we report the 0-shot result on both PubMed, MegMCQA, and MedQA datasets. Regarding the general instruction tuning scenario, we report 0-shot result on both SIQA and CommonsenseQA for LLaMA-3.1 8B, Mistral 7B, and Gemma-2 9B models. For the earlier-released LLaMA-2 7B model, since it has a shorter pre-training context length, we report its 5-shot result as Tulu 3 mainly enhances model performance with longer context.

**Prompt for Post-Training.** We employ the same prompt for post-training in both the medical domain and general instruction tuning scenario:

```
"Below is an instruction that describes a task, paired with an input that provides further context. Write a response that appropriately completes the request.\n\n### Instruction:\n{instruction}\n\n### Input:\n{input}\n\n### Response:\n{output}<EOS_TOKEN>"
```

We simply keep the instruction field empty if no instruction is provided.

<sup>1</sup>[https://huggingface.co/datasets/axiong/pmc.llama\\_instructions](https://huggingface.co/datasets/axiong/pmc.llama_instructions)

<sup>2</sup><https://huggingface.co/datasets/allenai/tulu-3-sft-mixture>

Table 7: Post-training performance comparison. **Bold** and underline denote the best and second-best performance of compressed models. For each method, we report their time to first token (TTFT, in seconds) and KV-cache retain rate (KV Cache).

| Method                     | TTFT (s) | KV Cache | Medical     |             |             |             | General     |               |             |
|----------------------------|----------|----------|-------------|-------------|-------------|-------------|-------------|---------------|-------------|
|                            |          |          | PubMedQa    | MedMCQA     | MedQA       | AVG         | SIQA        | CommonsenseQA | AVG         |
| <b>Mistral-7B (w/ GQA)</b> |          |          |             |             |             |             |             |               |             |
| Pre-Trained                | 1.94     | 100%     | 75.8        | 48.3        | 50.9        | 58.3        | 46.7        | 56.5          | 51.6        |
| Post-Train                 | 1.94     | 100%     | 78.8        | 49.7        | 60.3        | 62.9        | 53.7        | 76.6          | 65.2        |
| LLMDrop-Half               | 1.54     | 81.3%    | 78.0        | 50.6        | <u>59.0</u> | 62.5        | <u>52.5</u> | 74.5          | 63.5        |
| LLMDrop-Full               | 1.21     | 62.5%    | <b>79.0</b> | 50.2        | 56.7        | 62.0        | 51.8        | 73.6          | 62.7        |
| CLA-Half                   | 1.94     | 81.3%    | 78.6        | <u>56.0</u> | 58.5        | <u>64.4</u> | 52.0        | <b>77.9</b>   | <u>65.0</u> |
| CLA-Full                   | 1.91     | 62.5%    | <u>78.8</u> | 55.0        | 55.0        | 62.9        | 50.5        | 75.1          | 62.8        |
| UniAttn                    | 1.23     | 81.3%    | 78.2        | <b>57.3</b> | <b>60.5</b> | <b>65.3</b> | <b>53.4</b> | <u>77.5</u>   | <b>65.5</b> |
| <b>Gemma2-9B (w/ GQA)</b>  |          |          |             |             |             |             |             |               |             |
| Pre-Trained                | 2.23     | 100%     | 78.6        | 57.6        | 60.6        | 65.6        | 51.5        | 68.4          | 60.0        |
| Post-Train                 | 2.23     | 100%     | 78.6        | 58.6        | 61.9        | 66.4        | 54.4        | 75.6          | 65.0        |
| LLMDrop-Half               | 1.94     | 81.0%    | 78.6        | 56.4        | <u>60.5</u> | <u>65.2</u> | <b>55.6</b> | 68.4          | 62.0        |
| LLMDrop-Full               | 1.66     | 64.3%    | 78.2        | 54.8        | 58.7        | 63.9        | <u>54.8</u> | 62.9          | 58.9        |
| CLA-Half                   | 2.19     | 78.6%    | <b>79.2</b> | <u>56.6</u> | 56.3        | 64.0        | 53.5        | <b>76.0</b>   | <b>64.8</b> |
| CLA-Full                   | 2.24     | 64.3%    | 74.0        | 39.3        | 38.5        | 50.6        | 48.3        | 51.8          | 43.4        |
| UniAttn                    | 1.69     | 82.1%    | <u>79.0</u> | <b>60.7</b> | <b>64.3</b> | <b>68.0</b> | 53.7        | <u>74.4</u>   | <u>64.1</u> |

Table 8: Performance comparison (%) of different compensation designs.

| Input to $W_c$                | Output adds to          | AVG         |
|-------------------------------|-------------------------|-------------|
| MHA input                     | MHA output              | <b>65.4</b> |
| MHA input                     | FFN output              | 64.1        |
| MHA input                     | Activation before $W_o$ | <u>65.1</u> |
| Activation projected by $W_v$ | Activation before $W_o$ | 64.3        |

## B More Experiment Results

**Main Results on Mistral 7B and Gemma-2 9B.** We adopt the settings in Table 1 and conduct the same experiments on Mistral 7B (Jiang et al., 2023) and Gemma-2 9B (Rivière et al., 2024). The results are shown in Table 7. Consistent with the results on the LLaMA models, our UniAttn achieves the best overall performance on both LLMs and post-training datasets while significantly reducing both time and memory costs. When operating the same number of layers, UniAttn achieves similar TTFT time to LLMDrop, well demonstrating the effectiveness of Softmax activation unification. Although CLA and LLMDrop achieve competitive results in some settings (e.g., CLA-Half in post-training Gemma on general instruction datasets), *they cannot provide consistent performance across different settings*. Additionally, even on the Mistral and Gemma models, CLA achieves similar performance to its corresponding LLMDrop setting, again indicating that CLA diminishes the depth factor in pre-trained LLMs.

**Different Compensation Designs.** To compare different compensation designs, we attach the input and output of the  $W_c$  transformation to different activations. As shown in Table 8, directly compensating the MHA output with its input yields the best results. When adopting “finer compensation granularities”, i.e., positioning the input and output closer together (Rows 3 and 4), post-training performance decreases. Similarly, adopting “coarser compensation granularities”, i.e., moving the output compensation to after the FFN (Row 2), also results in lower performance. These findings suggest that using a linear transformation to compensate for errors specifically within the MHA module is the optimal approach. This aligns with our analysis in Section 3.3, which shows that the compensation error within the MHA module is significantly smaller in magnitude than its expectation.

**Experimental Analysis on the Impact of Model Depth.** In Section 3.4, we demonstrated that, unlike cross-layer KV sharing methods, UniAttn does not diminish the depth factor in pre-trained LLMs. To provide experimental evidence for this, we further apply LLMDrop to the MHA modules that utilize unified Softmax activations from preceding layers (a total of 12 layers in UniAttn for the LLaMA-3.1 8B model) in post-trained UniAttn models.

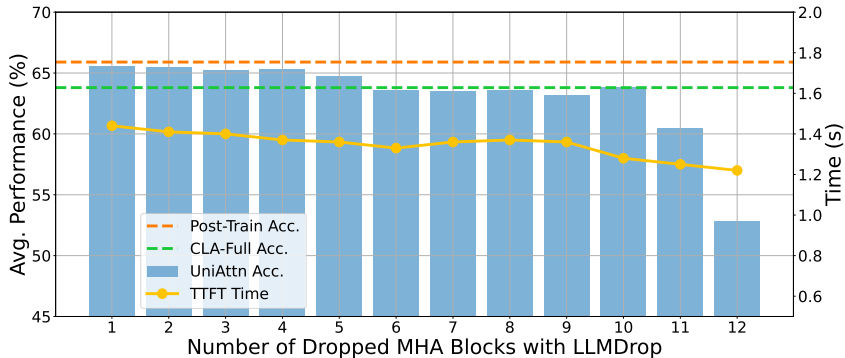


Figure 5: Results on further dropping UniAttn layers (%). We present the average accuracy and time to first token (TTFT) latency under different number of dropped MHA blocks via LLMDrop. Note that we only drop MHA blocks with unified Softmax activations.

Table 9: Performance (%) comparison with similarity-based Superblock grouping methods.

| Method  | Similarity Based Grouping | # of Operating Layers | PubMedQA | MedMCQA | MedQA | AVG  |
|---------|---------------------------|-----------------------|----------|---------|-------|------|
| UniAttn | ×                         | 3                     | 78.2     | 59.2    | 62.1  | 66.5 |
|         | √                         | 3                     | 77.6     | 57.3    | 57.8  | 64.2 |
| UniAttn | ×                         | 6                     | 77.2     | 58.1    | 62.9  | 66.1 |
|         | √                         | 6                     | 72.0     | 55.6    | 58.8  | 62.1 |
| UniAttn | ×                         | 9                     | 77.4     | 56.5    | 60.4  | 64.8 |
|         | √                         | 9                     | 77.4     | 54.2    | 56.0  | 62.5 |
| UniAttn | ×                         | 12                    | 79.0     | 57.6    | 59.5  | 65.4 |
|         | √                         | 12                    | 77.0     | 55.9    | 54.8  | 62.6 |

Specifically, we compute the input-output similarities of these MHA modules and simply prune the top  $k$  MHA modules with the highest similarities. The pruned model is then directly evaluated without additional fine-tuning. The average performance w.r.t.  $k$  is shown in Figure 5. As shown in the figure, pruning a few MHA modules from our UniAttn model still results in higher performance than the CLA-Full model variant. After pruning 10 MHA modules, UniAttn+LLMDrop achieves an average performance of 63.8, matching the performance of CLA-Full reported in Table 1. This demonstrates that UniAttn better preserves the impact of model depth compared to CLA. Furthermore, we can also conclude that the depth of the model significantly contributes to the post-train performance, thereby validating our theoretical analysis.

**Similarity-based Superblock Grouping.** We employed a simple fixed grouping method for Superblock construction, grouping every 4 layers in the *top half layers* as a Superblock. To investigate the impact of different Superblock grouping strategies, we experimented with a similarity-based grouping scheme. In this scheme, layers with the most similar Softmax activations, as measured by cosine similarity (Figure 2), are grouped together, and a linear compensation matrix is added to layers utilizing activations from other layers. As shown in Table 9, the similarity-based grouping consistently underperforms the fixed-size Superblock grouping (default implementation) across all settings. This suggests that the simple fixed-size Superblock approach is sufficient to achieve strong post-training performance.

### C Pipeline for Applying UniAttn during Post-Training

We provide a detailed pipeline for applying UniAttn as Algorithm 1.

**Algorithm 1** UniAttn Pipeline

---

**Input:** Pre-trained Model  $M$ , Post-train dataset  $D$ , SuperBlock size  $b$ , Apply SuperBlock merging from layer  $i_s$  to  $i_e$

Create UniAttn model  $M_{\text{uni}}$  by creating  $\frac{i_e - i_s + 1}{b}$  SuperBlocks in  $M$

Sample a subset  $D_{\text{init}}$  with 1000 samples from  $D$

For model  $M$ , forward all samples from  $D_{\text{init}}$ , calculate the average output activations  $\mathbf{x}'_i$  for each MHA block.

**for**  $i = 1$  **to**  $\frac{i_e - i_s + 1}{b}$  **do**

**for**  $j = 1$  **to**  $b - 1$  **do**

    For model  $M_{\text{uni}}$ , forward all samples from  $D_{\text{init}}$ , calculate the average output activations  $\mathbf{x}'_{\text{uni}, i_s + (i-1)b + j}$  and the average input activations  $\mathbf{x}_{\text{uni}, i_s + (i-1)b + j}$  for MHA block in layer  $i_s + (i - 1)b + j$ .

    Calculate the optimal initialization for the  $W_c$  matrix in layer  $i_s + (i - 1)b + j$  according to Theorem 3.7.

    Insert the initialized  $W_c$  matrix to layer  $i_s + (i - 1)b + j$  in model  $M_{\text{uni}}$ .

**end for**

**end for**

Freeze all training parameters other than the  $W_c$  matrices in  $M_{\text{uni}}$ . Train  $W_c$  with dataset  $D$  and apply early stop when loss stops to decrease (we consider the exponential moving average of training loss).

Conduct full fine-tune on  $M_{\text{uni}}$  with  $D$ .

**Output:** Trained UniAttn model  $M_{\text{uni}}$ .

---

**D Proof for Lemma 3.1**

*Proof.* Unroll the expression of  $\mathbf{x}_L$  and inductively:

$$\mathbf{x}_L = \mathbf{x}_0 + \sum_{k=1}^L F_k(\text{Norm}(\mathbf{x}_{k-1})) \quad (17)$$

As  $\|\text{Norm}(\mathbf{x}_k)\| = 1$  for all  $k$ , then:

$$\begin{aligned} \|\mathbf{x}_L\| &= \|\mathbf{x}_0 + \sum_{k=1}^L F_k(\text{Norm}(\mathbf{x}_{k-1}))\| \\ &\leq \|\mathbf{x}_0\| + \sum_{k=1}^L \|F_k(\text{Norm}(\mathbf{x}_{k-1}))\| \\ &\leq \|\mathbf{x}_0\| + \sum_{k=1}^L \|\lambda \cdot \text{Norm}(\mathbf{x}_{k-1})\| \\ &= \|\mathbf{x}_0\| + \lambda L \end{aligned} \quad (18)$$

□

**E Insights for Assumption 3.5**

With Lemma 3.1 and Proposition 3.2, we have shown that pre-trained Pre-Norm LLMs can be approximated as linear Pre-Norm systems. Suppose a pre-trained LLM operates on activations  $\mathbf{x} \in \mathbb{R}^d$ , each layer  $i$  in the pre-trained LLM can be treated as a linear transformation matrix  $W_i \in \mathbb{R}^{d \times d}$ . A generic gradient-based update can be expressed as:

$$W_i^{t+1} = W_i^0 - \sum_{t=0}^t \eta \nabla_{W_i} \mathcal{L}^t \quad (19)$$

Hence, the norm between initial and final weights satisfies:

$$\|W_i^{t+1} - W_i^0\| \leq \sum_{t=0}^t \|\eta \nabla_{W_i} \mathcal{L}^t\| \quad (20)$$



We denote the singular value decomposition of  $W_i^{t+1} - W_i^0$  as  $W_i^{t+1} - W_i^0 = U\Sigma V^T$ , it is easy to derive that:

$$\|W_i^{t+1} - W_i^0\| = \sqrt{\text{tr}[(\|W_i^{t+1} - W_i^0\|)(\|W_i^{t+1} - W_i^0\|)^T]} = \sqrt{\text{tr}(U\Sigma V^T V \Sigma^T U^T)} = \sqrt{\text{tr}(\Sigma \Sigma^T)} = \sqrt{\sum_{i=1}^d \sigma_i^2} \quad (21)$$

where  $\sigma_i$  denote the  $i$ -th singular value in  $\Sigma$ . Normally, the largest singular value  $\sigma_{\max}$  dominates in the quadratic term, thus we can further write:

$$\|W_i^{t+1} - W_i^0\| = \sqrt{\sum_{i=1}^d \sigma_i^2} \approx \sigma_{\max}(W_i^{t+1} - W_i^0) \quad (22)$$

Based on the basic features of singular values, we can show that:

$$\sigma_{\max}(W_i^{t+1}) \leq \sigma_{\max}(W_i^0) + \sigma_{\max}(W_i^{t+1} - W_i^0) \leq \sum_{t=0}^t \|\eta \nabla_{W_i} \mathcal{L}^t\| + \sigma_{\max}(W_i^0) \quad (23)$$

Due to having smaller values of  $\|\eta \nabla_{W_i} \mathcal{L}^t\|$  (i.e., smaller gradient norm), compared to earlier layers, the top layers typically have smaller updates on the largest singular value, thus tend to have smaller  $\sigma_{\max}$  values. This further leads to Assumption 3.5 we propose in the article.

## F Proof for Theorem 3.7

*Proof.* Solving for the optimal initialization of  $W_c$  is equivalent to solving the following optimization problem:

$$\min_{W_c} \|\mathbb{E}(\mathbf{x}_{i+b} W_c - \epsilon)\|^2 \quad (24)$$

Since  $W_c$  is the fixed weight of the linear transformation applied to input,  $W_c$  is independent of  $\mathbf{x}_{i+b}$ . Therefore, we can re-write the optimization problem as:

$$\min_{W_c} \|\mathbb{E}(\mathbf{x}_{i+b}) W_c - \mathbb{E}(\epsilon)\|^2 \quad (25)$$

The solution to the above system is given by  $W_c = \mathbb{E}(\mathbf{x}_{i+b})^+ \mathbb{E}(\epsilon)$ , where  $\mathbb{E}(\mathbf{x}_{i+b})^+$  denotes the Moore–Penrose inverse of  $\mathbb{E}(\mathbf{x}_{i+b})$ . By plugging in the closed-form expression of  $\mathbb{E}(\mathbf{x}_{i+b})^+$ , we achieve:

$$W_c = V \Sigma^+ U^T \mathbb{E}(\epsilon), \quad (26)$$

where  $\mathbb{E}(\mathbf{x}_{i+b}) = U \Sigma V^T$  denotes the SVD decomposition of  $\mathbb{E}(\mathbf{x}_{i+b})$ .  $\square$

## G More Insights on Linear Compensation

To demonstrate the effectiveness of our linear compensation strategy, we propose the following theorem:

**Theorem G.1.**  $A, B \in \mathbb{R}^{m \times n}$ ,  $X \in \mathbb{R}^{n \times n}$ . Suppose that each element from  $A$  and  $B$  are drawn from a Gaussian distribution such that  $a_{ij}, b_{ij} \sim N(0, 1)$ . It satisfies that:

$$\mathbb{E}[\min_X \|AX - B\|] = \begin{cases} \sqrt{n(m-n)}, & \text{if } m \geq n, \\ 0, & \text{if } m < n. \end{cases} \quad (27)$$

See the following subsections for the proof. In the article, we apply the F15K dataset (Su, 2023) to calculate the error  $\epsilon$  on LLaMA-2 7B (Touvron et al., 2023) and LLaMA-3.1 8B (Dubey et al., 2024) models after inserting the initialized linear transformation  $W_c$  according to Theorem 3.7. While the sequence length being  $m = 5120$  and the hidden size of applied models being  $n = 4096$ , the error is 11.09 and 5.76 after linear compensation, correspondingly, which are both *magnitudes lower* than their expectations on random data. Those results demonstrate the effectiveness of our linear compensation strategy.

We give the proof for Theorem G.1 in the following subsections.

## G.1 Preliminaries

To prove Theorem G.1, we adopt the notations in Theorem G.1 and prove a series of lemmas first.

**Lemma G.2.** *Let  $P = AA^+$ ,  $P$  is an orthogonal projection and  $\text{Im}(P) = \text{Col}(A)$ .*

*Proof.* The Moore-Penrose inverse matrix exhibits some basic features, namely  $AA^+A = A$  and  $(AA^+)^T = AA^+$ . Using that feature we can easily verify that:

$$P^2 = AA^+AA^+ = (AA^+A)A^+ = AA^+ = P \quad (28)$$

$$P^T = (AA^+)^T = AA^+ = P \quad (29)$$

So  $P$  is an orthogonal projection.

Next, we prove  $\text{Im}(P) = \text{Col}(A)$ . For any vector  $\mathbf{v} \in \text{Col}(A)$ , there exists a  $\mathbf{c} \in \mathbb{R}^n$  that  $\mathbf{v} = A\mathbf{c}$ . We have:

$$P\mathbf{v} = AA^+A\mathbf{c} = (AA^+A)\mathbf{c} = A\mathbf{c} = \mathbf{v} \quad (30)$$

So  $\mathbf{v} \in \text{Im}(P)$ . Therefore,  $\text{Col}(A) \subseteq \text{Im}(P)$ . Since  $P = AA^+$ , it is obvious that  $\text{Im}(P) \subseteq \text{Col}(A)$ . Hence, we can conclude that  $\text{Im}(P) = \text{Col}(A)$ .  $\square$

**Lemma G.3.**  *$I - P$  is an orthogonal projection and  $\text{Im}(I - P) = \text{Col}(A)^\perp$ .*

*Proof.* First, we prove that  $I - P$  is an orthogonal projection:

$$(I - P)^2 = I - 2P + P^2 = I - 2P + P = I - P \quad (31)$$

$$(I - P)^T = I - P^T = I - P \quad (32)$$

Then, we prove that  $\text{Im}(I - P) = \text{Col}(A)^\perp$ . For any  $\mathbf{v} \in \text{Im}(I - P)$ , there exists a  $\mathbf{c} \in \mathbb{R}^m$  that  $\mathbf{v} = (I - P)\mathbf{c}$ . Let  $\mathbf{d} \in \text{Col}(A)$ , then there exists a  $\mathbf{w} \in \mathbb{R}^n$  that  $\mathbf{d} = A\mathbf{w}$ . Computing the inner product of  $\mathbf{v}$  and  $\mathbf{d}$  yields:

$$\langle \mathbf{v}, \mathbf{d} \rangle = \langle (I - P)\mathbf{c}, A\mathbf{w} \rangle = \langle \mathbf{c}, (I - P)A\mathbf{w} \rangle = \langle \mathbf{c}, (A - AA^+A)\mathbf{w} \rangle = \langle \mathbf{c}, \mathbf{0} \rangle = 0 \quad (33)$$

This shows that  $\mathbf{v} \in \text{Col}(A)^\perp$ , and in turn  $\text{Im}(I - P) \subseteq \text{Col}(A)^\perp$ .

Conversely, suppose  $\mathbf{u} \in \text{Col}(A)^\perp$ . Recall Lemma G.2 that  $P$  is an orthogonal projection and  $\text{Im}(P) = \text{Col}(A)$ , we have  $P\mathbf{u} = \mathbf{0}$ . Therefore,

$$(I - P)\mathbf{u} = \mathbf{u} - P\mathbf{u} = \mathbf{u} \quad (34)$$

This shows that  $\mathbf{u} \in \text{Im}(I - P)$ , and in turn  $\text{Col}(A)^\perp \subseteq \text{Im}(I - P)$ . Therefore,  $\text{Im}(I - P) = \text{Col}(A)^\perp$ .  $\square$

From Lemma G.3, we can immediately conclude that:

**Corollary G.4.**  $\text{rank}(I - P) = m - \min(m, n)$

*Proof.*  $\text{rank}(I - P) = \dim \text{Im}(I - P) = \dim \text{Col}(A)^\perp = m - \text{rank}(A)$ . Recall Theorem G.1 that every element from  $A$  is sampled from a Gaussian distribution, so that by probability of 1 we have  $\text{rank}(A) = \min(m, n)$ , which leads to the conclusion of this corollary.  $\square$

Lastly, we give a lemma on orthogonal projections to a Gaussian-sampled vector:

**Lemma G.5.** *If  $\mathbf{b} \sim N(\mathbf{0}, I_{m \times m})$  is a standard Gaussian in  $\mathbb{R}^m$  and  $Q$  is an orthogonal projector of rank  $k$ , then*

$$\mathbb{E}[\|\mathbf{Q}\mathbf{b}\|] = \sqrt{k} \quad (35)$$

*Proof.*  $\mathbb{E}[\|\mathbf{Q}\mathbf{b}\|^2] = \mathbb{E}[\mathbf{b}^T Q^T Q \mathbf{b}] = \mathbb{E}[\mathbf{b}^T Q \mathbf{b}] = \mathbb{E}[\text{tr}(\mathbf{b}^T Q \mathbf{b})] = \mathbb{E}[\text{tr}(Q \mathbf{b} \mathbf{b}^T)] = \text{tr}(Q \mathbb{E}[\mathbf{b} \mathbf{b}^T])$ . As  $\mathbf{b} \sim N(\mathbf{0}, I_{m \times m})$ ,  $\mathbb{E}[\mathbf{b} \mathbf{b}^T] = I$ . Therefore, using the trace property of projectors:

$$\text{tr}(Q \mathbb{E}[\mathbf{b} \mathbf{b}^T]) = \text{tr}(Q) = k \quad (36)$$

In turn, we can conclude that  $\mathbb{E}[\|\mathbf{Q}\mathbf{b}\|] = \sqrt{k}$ .  $\square$

## G.2 Proof

Finally, we give the proof for Theorem G.1.

*Proof.* According to Theorem 3.7, for given  $A$  and  $B$ , the optimal solution  $X^*$  that satisfies  $\|AX^* - B\| = \min_X \|AX - B\|$  is given by:

$$X^* = A^+B, \quad (37)$$

where  $A^+$  is the Moore-Penrose inverse of  $A$ . We can re-write the objective as:

$$\mathbb{E}(\|AA^+B - B\|^2) = \mathbb{E}(\|(I - AA^+)(-B)\|^2) = \mathbb{E}(\|(I - AA^+)B\|^2) = \sum_{i=1}^n \mathbb{E}(\|(I - AA^+)\mathbf{b}_i\|^2) \quad (38)$$

According to Lemma G.3 and Corollary G.4,  $I - AA^+$  is an orthogonal projection and  $\text{rank}(I - AA^+) = m - \min(m, n)$ . With Lemma G.5, we know that for any  $i$ ,  $\mathbb{E}(\|(I - AA^+)\mathbf{b}_i\|^2) = m - \min(m, n)$ . Therefore, we can conclude that:

$$\mathbb{E}(\|AA^+B - B\|^2) = \begin{cases} n(m - n), & \text{if } m \geq n, \\ 0, & \text{if } m < n. \end{cases} \quad (39)$$

which leads to the conclusion in Theorem G.1.  $\square$